



# Evapotranspiration over a processing cassava field: a comparative analysis of micrometeorological methods and remote sensing

Neilon Duarte da Silva<sup>1</sup> · Aureo Silva de Oliveira<sup>2</sup> · Maurício Antônio Coelho Filho<sup>3</sup>

Received: 23 November 2021 / Accepted: 30 April 2024 / Published online: 15 May 2024  
© The Author(s), under exclusive licence to Springer-Verlag GmbH Austria, part of Springer Nature 2024

## Abstract

The need for reliable evapotranspiration (ET) estimates has prompted the introduction of new methodologies. This study aimed at studying the ET of a processing cassava field (13°6'39" S, 39°16'46" W, 154 m asl) in a tropical climate in Bahia, Brazil, under rainfed conditions from April to August 2019 by means of micrometeorological and remote sensing methods. The combination of surface renewal analysis and energy balance (SREB) demonstrated its potential to accurately determine the crop ET once calibrated against eddy covariance measurements of H. Remote sensing techniques were also applied with the METRIC and SAFER algorithms. Due to frequent cloud cover in the area, only three Landsat images from overpasses in May and June could be used. High agreement in terms of crop ET was found between the surface and the remote sensing methods. For the three images processed, METRIC and SAFER were 8.6% and 26.4% higher than SREB, on average. Among the proposed regression models (M1, M2, and M3) for estimation of processing cassava ET, M3 showed a better adjustment with the highest coefficient of determination ( $r^2 = 0.952$ ) and lowest error (RMSE = 0.205 mm day<sup>-1</sup>). In the M3 model, ET/Rn was expressed as a function of the NDVI/LAI ratio. These three biophysical parameters, Rn, NDVI, and LAI, can routinely be determined from image processing for field applications in water management at the studied region. Therefore, with a limited set of variables, this approach can be satisfactorily applied using data collection methodologies that provide enhanced temporal and spatial resolution.

## 1 Introduction

In Brazil, cassava is grown all over the country. In 2017, the cultivated area encompassed 1.4 million hectares, with yields ranging from 9.8 to 21.9 tons ha<sup>-1</sup> and a national average of approximately 15 tons ha<sup>-1</sup> (Embrapa, 2018). A recent survey from IBGE (Brazilian Institute of Geography and Statistics) indicated, for the 2020/2021 season, an area of 1.32 million hectares and a production of 19.7 million

tons of roots. Cassava is predominantly grown under rainfed conditions, yet its yield can double when subjected to irrigation (Coelho Filho 2020).

High-quality meteorological data is imperative for accurate evapotranspiration (ET) estimates (Allen 1996), with ET representing a critical variable at the surface-atmosphere interface for quantifying water consumption of agricultural crops and natural vegetation. ET, by itself, is a complex hydrological process and its determination require reliable instrumentation and skilled personnel not only to adequately deploy the sensors and operate them but also to analyze the data. Methods for ET determination generally fall into three categories: mass balance (e.g., weighing lysimeters), energy balance (e.g., Bowen ratio) and aerodynamic methods (eddy covariance).

Although these techniques may generate "accurate" ET estimates within a homogeneous area, their extrapolation to a broader scale is impeded by the inherent land surface heterogeneity, the intricate nature of hydrological processes, and the requisite for an array of surface measurements and land surface parameters (Jensen and Allen 2016). The energy balance method ( $R_n = LE + H + G$ ), for example, offers a

✉ Neilon Duarte da Silva  
neilon.silva@ifpa.edu.br

Aureo Silva de Oliveira  
aureo@ufrb.edu.br

Maurício Antônio Coelho Filho  
mauricio-antonio.coelho@embrapa.br

<sup>1</sup> Instituto Federal de Ciência e Tecnologia do Pará, Belém, Brazil

<sup>2</sup> Universidade Federal do Recôncavo da Bahia, Cruz das Almas, Brazil

<sup>3</sup> Empresa Brasileira de Pesquisa Agropecuária (Embrapa), Cruz das Almas, Brazil

mathematically straightforward solution when focused on determining the latent heat flux (LE). However, the H component (sensible heat flux) poses significant challenges for its measurement or estimation. Determination of H has been commonly made with the eddy covariance technique (Burba 2013; Perez-Priego et al. 2017; Cao et al. 2018; Foltýnová et al. 2019;) and the surface renewal analysis, as originally proposed by Paw et al. (1995). Since then, surface renewal analysis has been extensively used for finding H in energy balance studies over many vegetated surfaces (Hu et al. 2018; McElrone et al. 2013; Parry et al. 2019).

Currently, a wide spectrum of approaches based on satellite observations has been developed for ET and water management studies in conjunction with traditional ground-based monitoring techniques. A landmark to make satellite products operational is the SEBAL algorithm (*Surface Energy Balance Algorithm for Land*) (Bastiaanssen et al. 1998a, b), which was followed by others models like SEBS (Su 2002) and METRIC (*Mapping ET with high Resolution and Internalized Calibration*) (Allen et al. 2007a, b). Teixeira, (2010) proposed a simplified approach with the SAFER algorithm (*Simple Algorithm For Evapotranspiration Retrieving*) for solving the energy balance from vegetation indices and surface temperature data.

The present report is part of larger study that was conducted on a field of processing cassava aiming at evaluating the exchange of heat and water vapor between the surface and the atmosphere. It is recognized the existence of a significant gap of information on cassava water requirements which can prevent the implementation of any irrigation scheduling approach for root yield optimization. In order to reach our goals in quantifying the cassava ET, sensors needed by the surface renewal analysis and eddy covariance were deployed. Additionally, satellite products were used to develop a simplified remote sensing procedure, resulting in an alternative method that demands a reduced amount of surface data.

## 2 Material and methods

### 2.1 Description of the experimental site

Fieldwork was conducted at the Novo Horizonte Farm (13°06'39"S, 39°16'46"W, 154 m asl), State of Bahia, Brazil. The farm belongs to a private company specialized in growing cassava cultivars for starch production as well as other food products. The region's climate is transitional between Af (tropical without dry season) and Am (monsoon tropical), according to the Köppen system (Alvares et al. 2013). The average annual temperature is around 24 °C, with an average of 70% for the annual relative humidity.

Table 1 lists the fast-response and slow-response sensors taken to the field for data collection. The main criterion for choosing a spot in the area for positioning the tower was to ensure sufficient upwind fetch. Micrometeorological methods usually demand a minimum fetch size for the measurements to be representative. The cassava field where the tower was deployed was around 19 ha of total area. The maximum upwind fetch (SSE direction) was not less than 500 m and a minimum of 80 m of the same crop was identified in all other directions from aerial images taken with an unmanned aerial vehicle.

Two CR1000 dataloggers (Campbell Scientific) were used to collect data. This was done at 10 Hz frequency for the fast response sensors, while with the low response sensors data were collected at every 10 s. Within the datalogger, data were then integrated to 30-min interval and used to solve the energy balance equation.

### 2.2 Determining the energy balance components

#### 2.2.1 Sensible heat flux

The sensible heat flux density was determined by two methods: (1) the surface renewal analysis (SR) and (2) the eddy

**Table 1** Fast and slow response instruments installed in the experimental plot

Instrument	Model	Manufacturer	Height or depth (cm)	Measured parameter
Fast response sensors				
3D sonic anemometer	81,000	RM Young	230	Wind velocity components and sonic temperature
Fine-wire thermocouple	FW3 ( $\phi$ 76 $\mu$ m)	Campbell Scientific	180	Air temperature
Slow response sensors				
Net radiometer	NRLite	Kipp & Zonen	270	Net radiation
Pyranometer	SPLite	Kipp & Zonen	270	Solar radiation
Heat flux plate	HFP01	Hukseflux	8	Ground heat flux
Soil thermocouple	TCAV	Campbell Scientific	2 and 6	Soil temperature
Soil moisture meter	GS1	Decagon Devices	4	Soil moisture

covariance technique (EC). The second was used as a reference for calibrating the first. Shortly, the surface renewal analysis requires measurements of rapid fluctuations of air temperature, typically in the range of 2 – 10 Hz, with a single unshielded fine-wire thermocouple. These measured fluctuations are then used to calculate the temperature ramp amplitude, which is one of the main inputs for H calculation according to Eq. 1. In the present study, the measurements were made at 10 Hz frequency.

$$H_{SR} = \alpha \cdot H' = \alpha \left[ \rho c_p \frac{A}{d+s} z \right] \tag{1}$$

where:  $H_{SR}$  is the sensible heat flux after calibration ( $W m^{-2}$ );  $H'$  is sensible heat flux before calibration ( $W m^{-2}$ );  $\alpha$  is a calibration factor;  $\rho$  is the air density ( $kg m^{-3}$ );  $c_p$  is the specific heat of air at constant pressure ( $J kg^{-1} \text{ } ^\circ C^{-1}$ );  $A$  is the ramp amplitude ( $^\circ C$ );  $1 / (d+s)$  is the ramp frequency ( $s^{-1}$ ); and  $z$  is the height of air temperature measurement (m).

Snyder et al. (1996), Mekhmandarov et al. (2012) and Holwerda et al. (2021) used statistical moments and the Van Atta (1977) structure-functions to calculate A and (d+s) characteristics of the mean ramp. This procedure was also adopted in the present reasearch. With the values of A and (d+s), 30-min average values of H' were calculated within the datalogger according to Eq. 1. A calibration of H' against a reference is recommended to correct for unequal heating or cooling from the soil surface to the measurement height (top of the air parcel) (Snyder et al. 1996; Zapata and Martínez-Cob, 2001, 2002). As a first approximation,  $\alpha$  was set equal to 1.

The mean ramp amplitude (A) is estimated by solving the following set of equations for real roots (Eq. 2 to 4).

$$A^3 + pA + q = 0 \tag{2}$$

$$p = 10 \cdot S^2(r) - \frac{S^5(r)}{S^3(r)} \tag{3}$$

$$q = 10 \cdot S^3(r) \tag{4}$$

where:  $p$  and  $q$  are constants;  $S^n$  is the Van Atta structured function as given in Snyder et al. (1996); and  $r$  is the time lag. The time lag is calculated as the ratio of a sample lag ( $j$ ) between data points and data gathering frequency ( $f$ ) (Snyder et al. 1996).

Once the ramp amplitude was known, the inverse of the ramp frequency (d+s) was calculated according to Eq. 5.

$$d+s = -\frac{A^3 \cdot r}{S^3(r)} \tag{5}$$

In the second method, H was obtained using the eddy covariance technique according to Eq. 6.

$$H_{EC} = \rho c_p \overline{w'T'} \tag{6}$$

where:  $H_{EC}$  is the sensible heat flux ( $W m^{-2}$ ) from eddy covariance;  $\rho$  is air density ( $kg m^{-3}$ );  $c_p$  is specific heat of air at constant pressure ( $J kg^{-1} \text{ } ^\circ C^{-1}$ );  $w'$  is the instantaneous deviation of the vertical wind speed around the mean ( $m s^{-1}$ ); and  $T'$  is the instantaneous deviation of the sonic anemometer temperature around the mean ( $^\circ C$ ).

As previously mentioned, the EC method was used to calibrate the SR analysis, and the actual calibration coefficient  $\alpha$  was obtained as the slope of a linear regression through the origin where  $H_{EC}$  (Y-axis) was plotted against  $H'$  (X-axis) (Shapland et al. 2012a b). After obtaining  $\alpha$ , the calibrated sensible heat flux  $H_{SR}$  was obtained according to Eq. 1.

### 2.2.2 Ground heat flux

The soil heat flux represents the energy exchange between the surface and the subsurface layers and it was calculated according to Eq. 7.

$$G = G_8 + C_s \left( \frac{T_{s(i)} - T_{s(i-1)}}{\Delta t} \right) z_s \tag{7}$$

where:  $G$  is the soil heat flux ( $W m^{-2}$ );  $G_8$  is the heat flux measured at 8 cm below the surface ( $W m^{-2}$ );  $T_{s(i)}$  and  $T_{s(i-1)}$  are the mean soil temperatures ( $^\circ C$ ) above the plate at the beginning and end of the time interval  $\Delta t$  (1800s), respectively;  $z_s$  is the installation depth of the heat flux plate (m); and  $C_s$  is the soil heat capacity ( $J m^{-3} \text{ } ^\circ C^{-1}$ ) calculated with Eq. 8.

$$C_s = 2.01 \cdot 10^6 \rho_s / 2.65 + 4.19 \cdot 10^6 \theta \tag{8}$$

where:  $\rho_s$  is the soil density ( $1.30 Mg m^{-3}$ );  $\theta$  is the soil moisture ( $m^3 m^{-3}$ ); and 2.65 is the particle density ( $Mg m^{-3}$ ).

### 2.2.3 Latent heat flux

The latent heat flux ( $W m^{-2}$ ) was obtained as a residual of the energy balance (Eq. 9) and it represents the energy exchange associated with the transfer of water from the evaporating surface.

$$LE = Rn - G - H \tag{9}$$

## 2.3 Reference Crop Evapotranspiration

In this study, REF-ET v. 4.1 (Allen, 2015) was used to calculate daily ET<sub>o</sub> via the FAO56 Penman–Monteith model as given in Eq. 10. Meteorological data from a regional weather station located at about 30 km southeast of the experimental

site was used as input in Eq. 10. This station is part of the network of INMET, the Brazilian National Institute of Meteorology.

$$ET_o = \frac{0.408\Delta(R_n - G) + \gamma\left(\frac{900}{T+273}\right)u_2(e_s - e_a)}{\Delta + \gamma(1 + 0.34u_2)} \quad (10)$$

where:  $ET_o$  is the reference crop evapotranspiration ( $\text{mm day}^{-1}$ );  $R_n$  is in  $\text{MJ m}^{-2} \text{ day}^{-1}$ ;  $G$  is in  $\text{MJ m}^{-2} \text{ day}^{-1}$  and where  $G=0$  for 24-h time steps;  $\Delta$  is the declination of the saturation vapor pressure curve ( $\text{kPa } ^\circ\text{C}^{-1}$ );  $u_2$  is the wind speed at 2 m height ( $\text{m s}^{-1}$ );  $T$  is the mean air temperature ( $^\circ\text{C}$ );  $e_s$  is the saturation vapor pressure in the atmosphere ( $\text{kPa}$ );  $e_a$  is the actual vapor pressure ( $\text{kPa}$ ); and  $\gamma$  is the psychrometric constant ( $\text{MJ kg}^{-1}$ ).

## 2.4 Crop coefficient

The determination of the crop coefficient of the processing cassava over the measurement period was calculated as the ratio between crop ET ( $ET_c$ ) and  $ET_o$ , according to Eq. 11.

$$K_c = \frac{ET_c}{ET_o} \quad (11)$$

where:  $K_c$  is the mean crop coefficient (dimensionless) and  $ET_c$  is the crop ET ( $\text{mm day}^{-1}$ ).

## 2.5 Remote sensing of evapotranspiration

Images from the Landsat-7, Landsat-8, and CBERS-4A satellites were used to estimate the crop ET during the measurement period by means of the METRIC and the SAFER models as well as regression equations adjusted to the experimental data.

### 2.5.1 Crop ET with METRIC

The METRIC algorithm, as proposed by Allen et al. (2007a, b) is a model derived from the first version of SEBAL. In this model, a series of calculations at pixel level is performed to solve the energy balance equation for ET. METRIC was primarily developed for estimating ET from irrigated crops in Southern Idaho, USA.

The METRIC model has been extensively used in ET and water management studies of a large spectrum of crops in different parts of the world (Folhes et al. 2009; Pôças et al. 2014; Tasumi 2019; Ortega-Salazar et al. 2021). A detailed comparison between SEBAL and METRIC, where the characteristics and applications of both models are highlighted can be found in Allen et al. (2011).

The net all-wave radiation in our METRIC implementation was calculated with Eq. 12.

$$R_n = (1 - \alpha_o)SW_i + LW_i - LW_o - (1 - \epsilon_o)LW_i \quad (12)$$

where:  $R_n$  is in  $\text{W m}^{-2}$ ;  $\alpha_o$  is the surface albedo (dimensionless);  $SW_i$  is the incoming flux of shortwave radiation ( $\text{W m}^{-2}$ );  $LW_i$  is the incoming flux of longwave radiation ( $\text{W m}^{-2}$ );  $LW_o$  is the outgoing flux of longwave radiation ( $\text{W m}^{-2}$ ); and  $\epsilon_o$  is the surface emissivity (dimensionless).

The soil heat flux was calculated according to Eq. 13, where the ratio  $G/R_n$  is a function of surface temperature, surface albedo ( $\alpha_o$ ), and a vegetation index.

$$\frac{G}{R_n} = (T_s - 273.15)(0.0038 + 0.0074\alpha_o)[1 - 0.98(NDVI)^4] \quad (13)$$

where:  $G$  is in  $\text{W m}^{-2}$ ;  $R_n$  is in  $\text{W m}^{-2}$ ;  $T_s$  is the surface temperature (K); and  $NDVI$  is the normalized vegetation index (dimensionless). Calculation of  $NDVI$  is made with spectral radiances at shortwave bands of satellite images.

The sensible heat flux was calculated following a one-dimension, aerodynamic, temperature-gradient based equation for heat transport at the surface-atmosphere interface (Eq. 14).

$$H = \rho \cdot c_p \cdot \frac{dT}{r_{ah}} \quad (14)$$

where:  $H$  is in  $\text{W m}^{-2}$ ;  $\rho$  is the air density ( $\text{kg m}^{-3}$ );  $c_p$  is the air specific heat at constant pressure ( $1004 \text{ J kg}^{-1} \text{ K}^{-1}$ );  $dT$  (K) is the temperature difference between two near-surface heights ( $z_1$  and  $z_2$ ); and  $r_{ah}$  is the aerodynamic resistance to heat transport ( $\text{s m}^{-1}$ ).

In Eq. 14 there two unknowns,  $r_{ah}$  and  $dT$ , and therefore, an explicit solution is not possible. METRIC uses an iterative procedure based on two anchor pixels (“cold” and “hot”), where reliable values for  $H$  can be estimated, and solve for  $dT$  that satisfies Eq. 14 given the aerodynamic roughness and wind speed at a given height. Buoyancy effects on  $r_{ah}$  are taken into account by means of the Monin-Obukhov length ( $L$ ) that is used to define stability conditions of the atmosphere in the iterative process.

In order to estimate  $dT$  at each pixel of the image, METRIC assumes a linear relationship between  $dT$  and  $T_s$  of that particular pixel (Eq. 15).

$$dT = b + a \cdot T_s \quad (15)$$

where:  $a$  and  $b$  are empirically determined constants for a particular image, calculated based on the “cold” and “hot” pixels, for which a value for  $H$  is known.

The final step of the algorithm is to calculate the amount of water transferred from the surface at the moment of satellite overpass. Therefore, an instantaneous value ET is determined according to Eq. 16.

$$ET_{inst} = 3600 \frac{LE}{\lambda} \tag{16}$$

where:  $ET_{inst}$  is the instantaneous ET rate (mm h<sup>-1</sup>), 3600 converts seconds to hour, and  $\lambda$  is the latent heat of vaporization (J kg<sup>-1</sup>), which is a function of pixel temperature ( $T_s$ ).

The next step in the METRIC implementation is the calculation of the reference ET fraction (EToF) as given in Eq. 17. The EToF is defined as the ratio of  $ET_{inst}$  (Eq. 16) to ETo (Eq. 10) at the time of the image, this one calculated with weather data from a nearby weather station presented in the area covered by the satellite image.

$$EToF = \frac{ET_{inst}}{ETo} \tag{17}$$

METRIC extrapolates ET from instantaneous (overpass time) values to daily values (Eq. 18) by assuming a constant EToF during the day.

$$ET_{24} = EToF \cdot ETo_{24} \tag{18}$$

where:  $ET_{24}$  is the surface evapotranspiration (mm day<sup>-1</sup>);  $EToF$  is the reference ET fraction (dimensionless), and  $ETo_{24}$  is the daily refence crop ET (mm day<sup>-1</sup>).

### 2.5.2 Crop ET with SAFER

The SAFER model originally presented by Teixeira (2010) is also based on remote sensing data, but it takes another approach compared to METRIC, in the sense that ET in SAFER is not obtained as the residual of the energy balance equation. The only remote sensing parameters used in SAFER are surface albedo, surface temperature, and the normalized vegetation index (NDVI). Equation 19 is the final step in the implementation of the SAFER algorithm.

$$\frac{ET}{ETo} = \exp \left[ a + b \left( \frac{T_s}{\alpha_o \cdot NDVI} \right) \right] \tag{18}$$

where:  $ET$  is the surface ET (mm day<sup>-1</sup>);  $ETo$  is the reference crop ET (mm day<sup>-1</sup>) calculated with Eq. 10;  $a$  and  $b$  are calibration coefficients;  $\alpha_o$  is the surface albedo (dimensionless);  $T_s$  is the surface temperature (°C); and  $NDVI$  is the normalized vegetation index (dimensionless).

In the present paper, 1.0 was used for the coefficient  $a$  in Eq. 18 (Hernandez et al. 2014; Coaguila et al. 2017) and -0.008 for the coefficient  $b$  (Teixeira, 2010). Then, the ratio (ET/ETo) was multiplied by the FAO56 Penman–Monteith ETo to obtain the current crop evapotranspiration (ETc).

This model has been calibrated and applied to diferentes regions of Brazil (Hernandez et al. 2014; Teixeira et al. 2015a, b, c). It has also recently tested with different versions of the PM equation based on the several combinations of missing weather data (Santos et al. 2020).

In the SAFER implementation, the NDVI was obtained from spectral radiances at shortwave bands while  $\alpha_o$  and  $T_s$  were estimated from linear regressions (Eq. 19 and 20).

$$\alpha_o = 0.61\alpha_{TOA} + 0.08 \tag{19}$$

$$T_s = 1.00T_{sat} - 20.17 \tag{20}$$

where:  $\alpha_{TOA}$  is the planetary albedo (dimensionless) and  $T_{sat}$  is the surface temperature at the thermal band of satellite image.

### 2.5.3 Proposed models for processing cassava ET estimation

This part presents a set of simplified models obtained through nonlinear regression routines within the XLSTAT analysis tool for Excel (Lumivero Inc). The basic idea behind the formulation of these proposed models (Eq. 21, 22, and 23) was to derive a crop ET calculation procedure that could be operational and sufficiently reliable at local level in the processing cassava farm as well as in regions whose climate pattern is similar.

The variables selected as input to the models (NDVI,  $R_n$ ,  $T_s$ , and LAI) have been extensively demonstrated to be associated with ET modelling over agricultural fields (Allen et al. 2007a, b; Teixeira, 2010) and natural vegetation (Sun et al. 2011).

$$M1 \quad ET = \exp \left\{ a \cdot \exp \left[ b \left( \frac{NDVI}{R_n} \right) + c \right] \right\} \tag{21}$$

$$M2 \quad \frac{ET}{R_n} = \exp \left[ a + b \left( \frac{NDVI}{T_s} \right) \right] \tag{22}$$

$$M3 \quad \frac{ET}{R_n} = \exp \left[ a + b \left( \frac{NDVI}{LAI} \right) \right] \tag{23}$$

where:  $a_1, a_2, a_3, b_1, b_2, b_3$ , and  $c$  are regression coefficients;  $ET$  is the cassava crop ET (mm day<sup>-1</sup>);  $R_n$  is in W m<sup>-2</sup>;  $LAI$  is the leaf area index (dimensionless); and  $T_s$  is in K.

All data used to adjust the above proposed models were obtained from the respective raster of each variable derived from satellite images while implementing the METRIC model. A two-step procedure was taken to adjust the models. Initially a set of pixels were sampled at different geographical coordinates across the raster images of the input variables with the aid of a 4.7-m resolution land-use map of the area (Fig. 1B) developed from a Planet satellite product (L15-0800E-0948N, June 2019) which was obtained from the Planet Labs website ([www.planet.com](http://www.planet.com)) (Fig. 1A). The second step consisted in sampling with an independent set of pixels for model validation.

Table 2 shows the quantitative of classes and the number of pixels used in calibrating and validating the models.



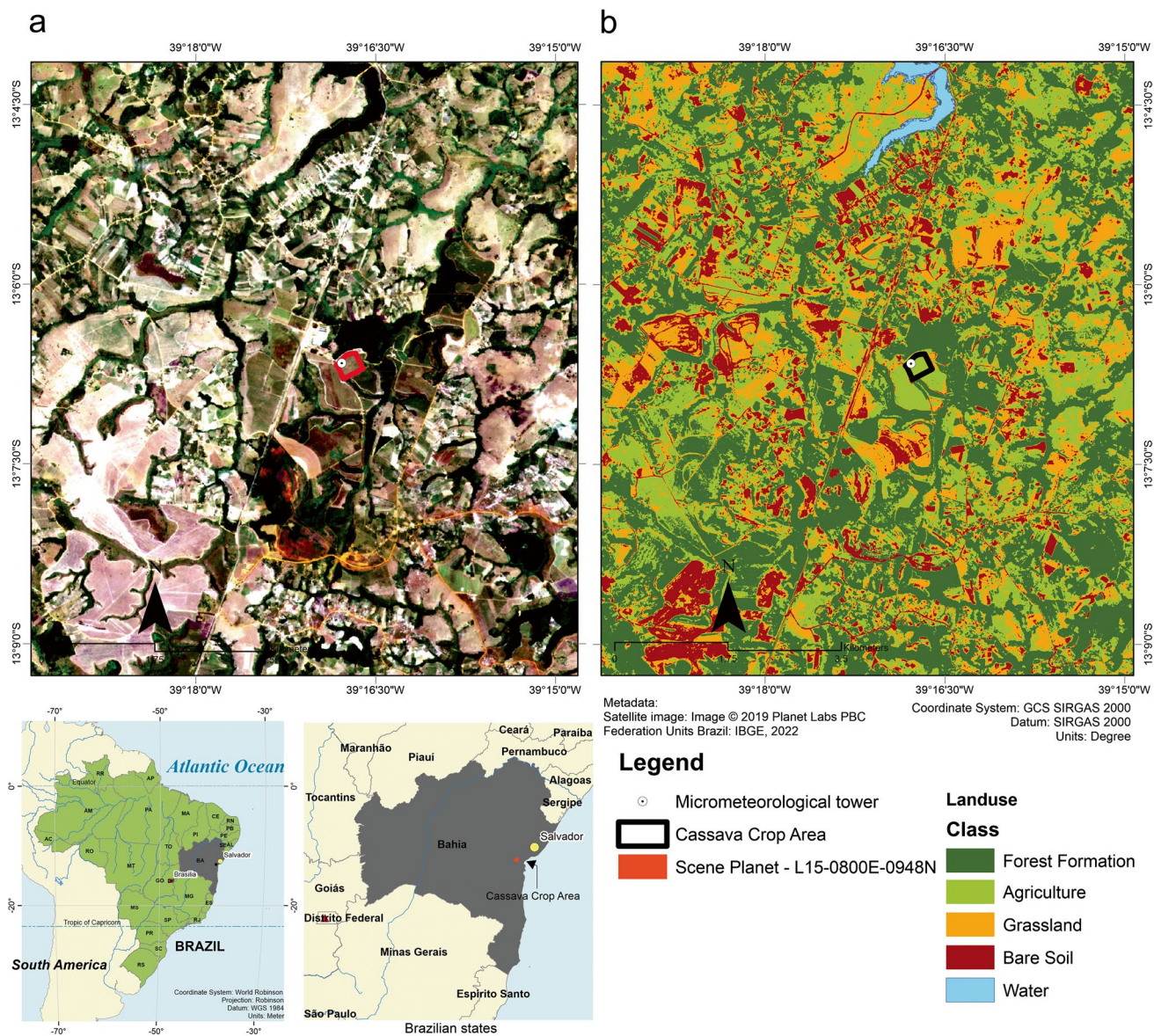


**Fig. 1** Original Planet satellite image (A) and the derived land use map (B) for pixel selection within the experimental area

For areas classified as agriculture/pastures, a more significant number of pixels were used in both steps of model formulation. The other quantities were divided based on the quality of the images of different dates to obtain a reasonable range of input variables (LE, Rn, Ts, NDVI, and LAI).

### 3 Results and discussion

#### 3.1 Energy Balance Components

Measurements of soil and atmospheric parameters in the cassava field spanned from April to August of 2019. During the months of May and June, during the vegetative stage, the

**Table 2** Land use classes and number of pixels sampled for calibration and validation of models M1, M2, and M3 for estimating processing cassava ET

Class	Area (ha)	Fraction (%)	Pixels for model calibration	Pixels for model validation
Bare soil	995.38	14.71	20	25
Agriculture	2871.26	42.43	180	200
Forest formation	1879.01	27.76	50	20
Water	406.75	6.01	30	20
Grassland	615.38	9.09	20	35
Total	6767.78	100	300	300

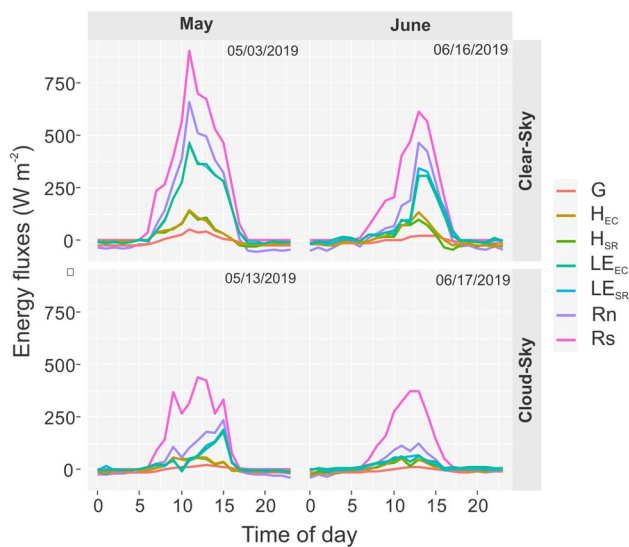


**Fig. 2** Hourly partition of energy balance components for different days in May and June for cloudy and clear sky conditions

crop covered the highest percentage of ground surface. Due to this, energy balance data from this period is emphasized under low and high cloud cover to exemplify the partitioning of the available energy.

The diurnal variations of these components for May and June are shown in Fig. 2. For this period, the maximum LE values were  $460.56 \text{ W m}^{-2}$  and  $332.45 \text{ W m}^{-2}$  observed on 05/03/2019 and 06/16/2019, respectively. From the data on global solar radiation ( $R_s$ ), days (13/05 and 17/06) different from those mentioned above were identified, these have high cloudiness, whose LE values represent the lowest for the period,  $180.34$  and  $65.23 \text{ W m}^{-2}$ . For 05/13/2019 and 06/17/2019, the sensible heat fluxes were practically equivalent to the heat flux into the soil, which indicates that there was less energy available to heat the air and the soil and that 90% of  $R_n$  was used for the process of losing water to the atmosphere, which agrees with Jensen and Allen (2016) and Gao et al. (2020).

A daily average of  $G$  was negative for both dates, 05/03/2019 and 06/16/2019, as observed in Fig. 2. Therefore, all the heat was released to the ground. The opposite situation occurred on the dates 05/13 and 05/17 when the most significant portion of  $R_s$  was not converted into LE, which represented about 17.45% and 14.34%, corresponding to an evaporative fraction [ $EF = LE/R_s$ ] around 56.72% and 51.95%, respectively. For 05/03/2019 and 06/16/2019, the highest available energy resulted in evaporative fractions of 79.64% and 69.22%, respectively.

Figure 3 shows the relationship between components of the energy balance in the processing cassava field from hourly averages of the data collected in the experimental area.

Figure 3A shows the relationship between soil heat flux ( $G$ ) and net radiation ( $R_n$ ). During the entire data collection period, which coincided with the vegetative phase of the cassava crop, the degree of ground cover was visually significant, especially because measurements started when the plants had an average height of 60 cm and a predominance of cloudy days. The average value found for the  $G/R_n$  ratio was only 6%, which is explained not only by the soil cover of the crop but also by the proliferation of weeds, considering that the crop was planted under rainy conditions. In addition to the change in soil water content, the type of cover is responsible for variations in soil heat flux.

Figure 3B shows the relationship between the sensible heat flux obtained via the eddy covariance method and the net radiation  $R_n$ . The average  $H/R_n$  ratio with this method was around 23%, indicating that most of the available energy was used for water evaporation, since  $LE/R_n$  ratio was around 71%, considering that the crop was conducted under rainfall conditions. Historically, the period from March to September is the wettest in the region, with over 70% of annual precipitation concentrated in these months.

From the point of view of partitioning of available energy for sensible heat flux, the values presented are consistent with those found by Lima et al. (2011) in research carried out with cowpea beans in dry conditions. The  $H/R_n$  ratio found by the authors ranged between 0.23 and 0.34. In a work field involving different types of soil coverages and associated with the cultivation of cassava, Attarod et al. (2005), using the Bowen ratio method, verified that at the closure of the energy balance, the  $LE/R_n$  ratio was 0.72 in periods with high water availability and 0.54 in periods of low water availability. According to Zhou et al. (2011), this high  $LE/R_n$  ratio is expected because without water restriction and with a high LAI (current crop phase, 150 DAP), there is an increase in transpiration, thus contributing to higher  $LE/R_n$  values and vice versa.

In an area of irrigated cotton during a period of high-water availability, Bezerra et al. (2015) found that the  $LE/R_n$  ratio was 0.70, with the highest values occurring when the soil was wetter. In their work, the authors verified that for two consecutive years (2008 and 2009), the  $G/R_n$  ratios were 10%, and for  $H/R_n$ , they were 17% in 2008 and 16% in 2009. Gao et al. (2020) compared evapotranspiration and energy partition related to vineyards main biotic and abiotic controllers using different irrigation methods. The authors found that the  $LE/R_n$  ratio was 0.75,  $H/R_n$  0.13, and  $G/R_n$  equal 0.12.

Similar values for another crop, beans, were reported by Lima et al. (2005), whose  $LE/R_n$  ratio was 0.71. Neves et al. (2008), in the opposite condition of water availability, when quantifying the energy balance components in cowpea beans, found mean values of  $LE/R_n$  equal to 0.21, mainly due to the low water availability throughout the crop cycle.



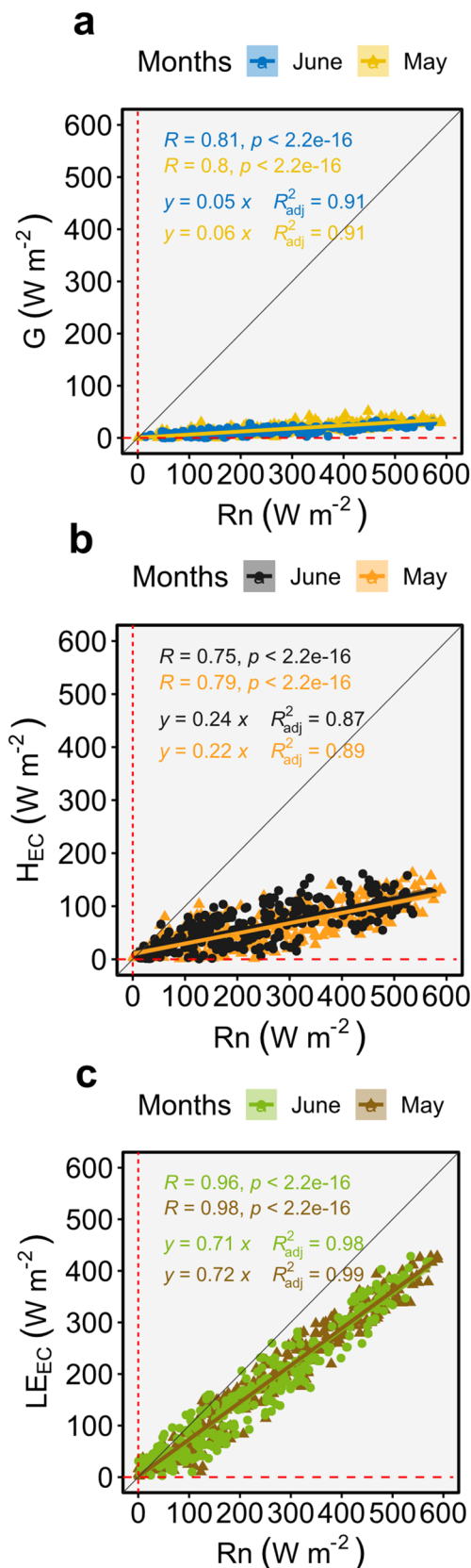


**Fig. 3** Relationship between the net radiation ( $R_n$ ) and the energy balance components ( $G$ ,  $H_{EC}$  and  $LE_{EC}$ )

### 3.2 Evapotranspiration of the processing cassava field

In the calibration of the surface renewal analysis for  $H$  estimation ( $H_{SR}$ ) a value of 0.96 was found for the calibration coefficient ( $\alpha$ ) as given in Eq. 1, with values ranging from 0.86 to 1.05 for all conditions of atmospheric stability.

The daily ET of processing cassava estimated with the energy balance based on  $H$  from the surface renewal analysis ( $H_{SR}$ ) and eddy covariance technique ( $H_{EC}$ ) is represented in Fig. 4. The ET values for both methods of  $H$  derivation ranged from 0.7 to 4.3 mm day<sup>-1</sup> with a total of 154.5 mm considering the entire measurement period made with the EC system and 160.0 mm obtained via the SR analysis. These totals express a daily difference of 0.09 mm day<sup>-1</sup>. The RMSE for the entire period was in the order of 0.185 mm day<sup>-1</sup>.

The mean value of  $K_c$  from  $ET_{EC}$  was, on average, in the order of 0.95, while the  $K_c$  calculated with  $ET_{SR}$  was 0.92 (Fig. 5). For the May and June period of 2019, the plants were with 150 DAP (days after planting), and  $K_c$  values for the period are consistent with those presented by Attarod et al. (2005) for a dryland cassava cultivation in Thailand. Recent data on cassava  $K_c$  in the eastern Bahia was reported by Coelho Filho (2020) whose values of  $K_c$  are compatible with those presented here; for a similar period, the average  $K_c$  was 0.98.

Under the argument of improving a methodology that would facilitate the estimates of crop coefficient, Koyo et al. (2020) used the NDVI to derive  $K_c$  for a cassava area in Benin, whose estimated values were based on those standardized by the FAO-56 (Allen et al. 1998). At the end of the final stage (210 DAP), the  $K_c$  estimated via NDVI had a higher value when compared to the FAO  $K_c$  for the same stage. Throughout the growth cycle, even for the periods of the first 20 days and between 60 and 150 DAP, during which the  $K_c$  of FAO-56 had constant values, that were similar to the present study, in the order of 0.98 in the root production stage.

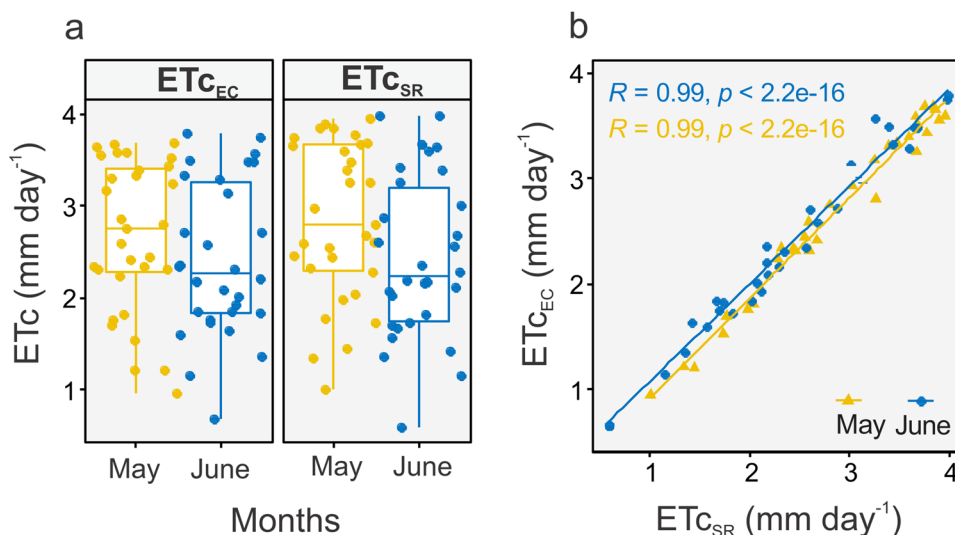
#### 3.2.1 Crop ET based on the remote sensing techniques

Table 3 shows the values of processing cassava ET from all surface (EC and SR) and remote sensing (METRIC and SAFER) methods. Compared to the surface methods the ET values obtained with the METRIC model were quite low, in the order of -0.316 and -0.180 mm for the EC and SR methods, respectively.

The tendency of overestimation of ET data is confirmed by other reports (González-Dugo et al. 2012; González-Piqueras et al. 2015). According to Bastiaanssen (2000), within the energy balance and when they involve remote sensing techniques, the heat flux in the soil ( $G$ ) is one of the main products that produce



**Fig. 4** Correlation between the processing cassava ET using the eddy covariance ( $ET_{EC}$ ) and the surface renewal analysis ( $ET_{SR}$ ) for May and June



**Fig. 5** Variation of processing cassava Kc obtained with SR analysis and EC sensible heat flux in the energy balance method

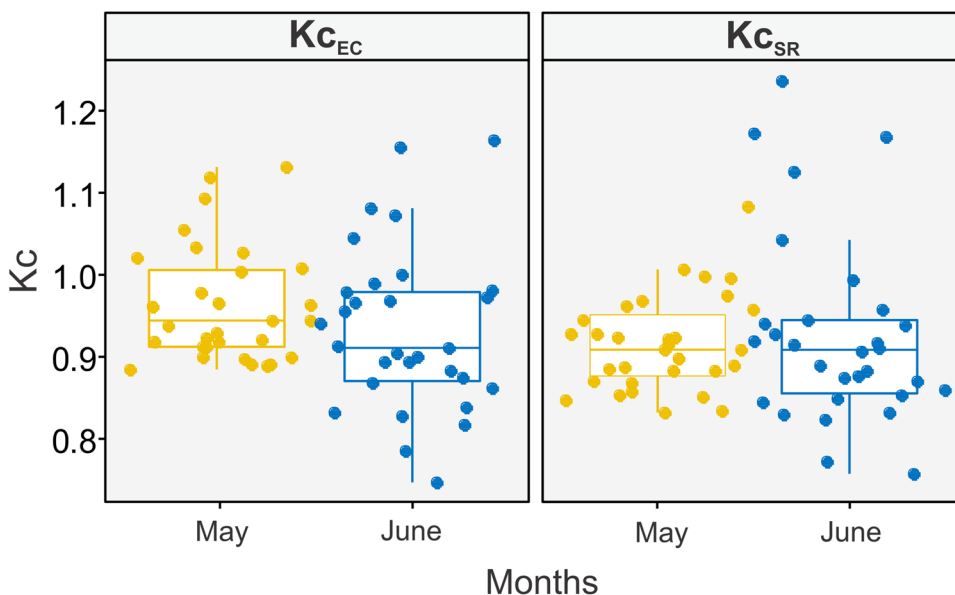


**Table 3** Processing cassava crop ET from surface (EC and SR) and remote sensing (METRIC and SAFER) methods

Satellite overpass date	EC ET (mm day <sup>-1</sup> )	SR ET (mm day <sup>-1</sup> )	METRIC	SAFER
05/24/2019	3.55	3.89	4.08	4.87
06/09/2019	2.21	2.17	2.55	2.93
06/25/2019	2.58	2.68	2.87	3.25
Mean	2.78	2.91	3.17	3.68

estimation errors, mainly when no map and ground cover are used. When not well identified, the type of coverage leads to unreliable estimates. As Boegh and Soegaard (2004) reported in a study carried out in Denmark, they combined NOAA AVHRR

data with the meteorological parameters generated by the weather forecast model to estimate ET. They pointed out that the method performed well under dense vegetation and favorable soil moisture conditions. However, the authors concluded that a correction must be made for dry regions for the decrease in ET caused by the difference in air temperature and vegetation surface temperature. It is worth noting that a use and coverage map helps refine the results and insert a local estimation methodology based on this information.

**3.2.2 Adjusted and validated models for crop ET estimation**

Figure 6A represents the direct relationship between ET and the NDVI/Rn ratio that expresses the influence of the degree of coverage on the available energy in the system.

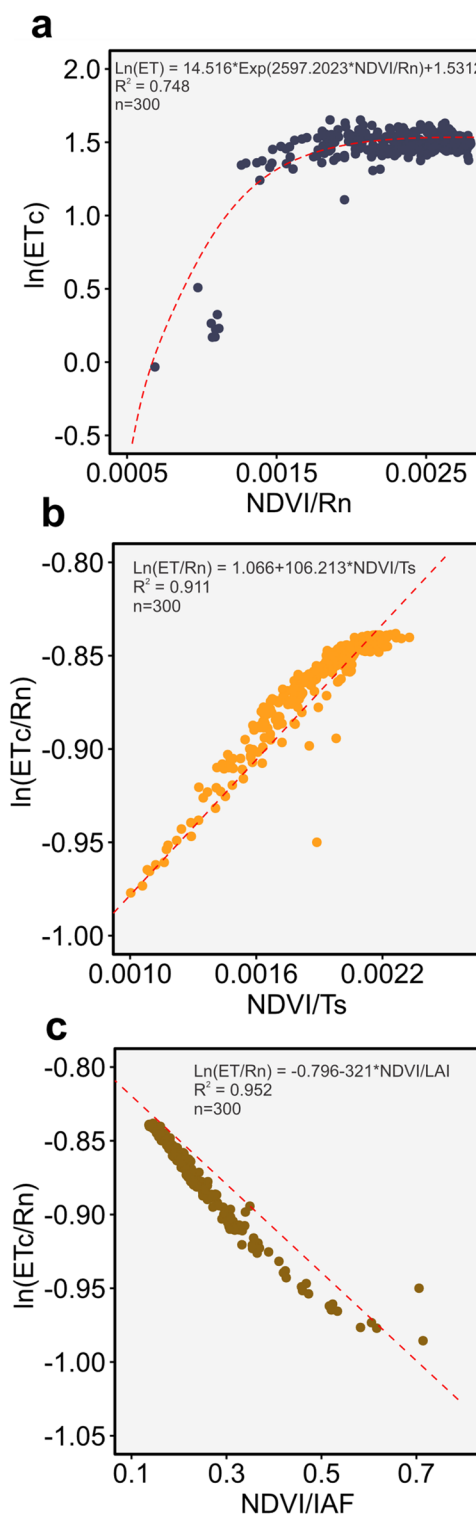
Figures 6B and 6C show the linear relationships between the ET/Rn ratio (which represents how much Rn was used for latent heat fluxes) and two other essential ratios, the NDVI/LAI, representing the relationship between vegetation vigor and the leaf area index and the NDVI/Ts then named by Karnieli et. al. (2010) from (Land Surface Temperature/NDVI) which has been used in various applications associated with surface water and energy balances. It is also associated with moisture availability and canopy resistance, indicating vegetation stress and soil water stress, which was previously reported by Gillies et al. (1997).

Table 4 presents the adjustment coefficients for the models observed in Fig. 7. The determination coefficients in Figs. 6B and C are satisfactory ( $R^2 > 0.90$ ). The model proposed in Fig. 6A was the one with the smallest  $R^2$ , followed by the highest RMSE in the order of 0.413 mm and 0.259 and 0.205 mm for the models in Figs. 6B and C, respectively. Despite the small number of valid images, the deviations are caused by some ET sensitivity analysis errors in remote sensing studies, as reported by Teixeira (2010) in a similar analysis.

The model expressing ET/Rn as a function of the NDVI/LAI ratio (M3) showed the smallest error in the estimate of ET compared to the one that uses the NDVI/Ts ratio (M2) for the overpass date of 06/29/2019 deviations of 0.33 and 0.16 mm and -0.30 to 0.020 mm. In this scenario in the spatial analysis, the model predicted, at worst, 70% of the estimates. These differences in the values of the deviations are mainly due to the variation of the LAI values, considering that the METRIC model predicts a maximum value of LAI in the order of 6. The insertion of this methodology with drones, associated with reduced and higher flight height spatiotemporal resolution, can reduce this deviation through a more accurate LAI with a wider range of values.

Focusing on NDVI data, a greater refinement in the quantities regarding negative values (water bodies or exposed soil) can vary the correlation of correct answers since the proposal is to compose a model for areas with vegetation cover. The vegetation cover responds with NDVI values ranging from 0.09 to 0.96, depending on its architecture, density, and moisture; therefore, the highest NDVI values are associated with areas of vegetation with greater vigor. Parallel to this analysis, using SAVI allows for a more robust analysis, given the high values of NDVI, while the numerical quantities of SAVI represent the same surface targets. However, with a different refinement, the denser the vegetation the better is the performance by the SAVI index is in distinguishing vegetation with high photosynthetic vigor from areas of bare soil.

For the model that expresses ET/Rn as a function of the NDVI/Ts ratio, on the overpass date of 06/09/2019, the deviations ranged between -0.45 and -0.185 mm and -0.37 to -0.016 mm for the overpassing date of 06/29/2019, respectively.



**Fig. 6** Plot of regression models M1, M2, and M3 for estimation of processing cassava ET

The uniformity of the cultivation area (whether at nutritional or soil moisture level) of cassava is responsible for the low variation in surface temperature, and this limits the model's

**Table 4** Coefficients of M1, M2, and M3 regression models for estimation of processing cassava crop evapotranspiration

Parameter	Model	Equation	Coefficients			R <sup>2</sup>	RMSE (mm)
			a	b	c		
ETc	M1	$exp\left\{a \cdot exp\left[b\left(\frac{NDVI}{R_n}\right) + c\right]\right\}$	14.516	2597.203	1.531	0.748	0.413
ETc/Rn	M2	$exp\left[a + b\left(\frac{NDVI}{T_s}\right)\right]$	-1.066	106.216	-	0.911	0.259
ETc/Rn	M3	$exp\left[a + b\left(\frac{NDVI}{LAI}\right)\right]$	-0.796	-0.321	-	0.952	0.205

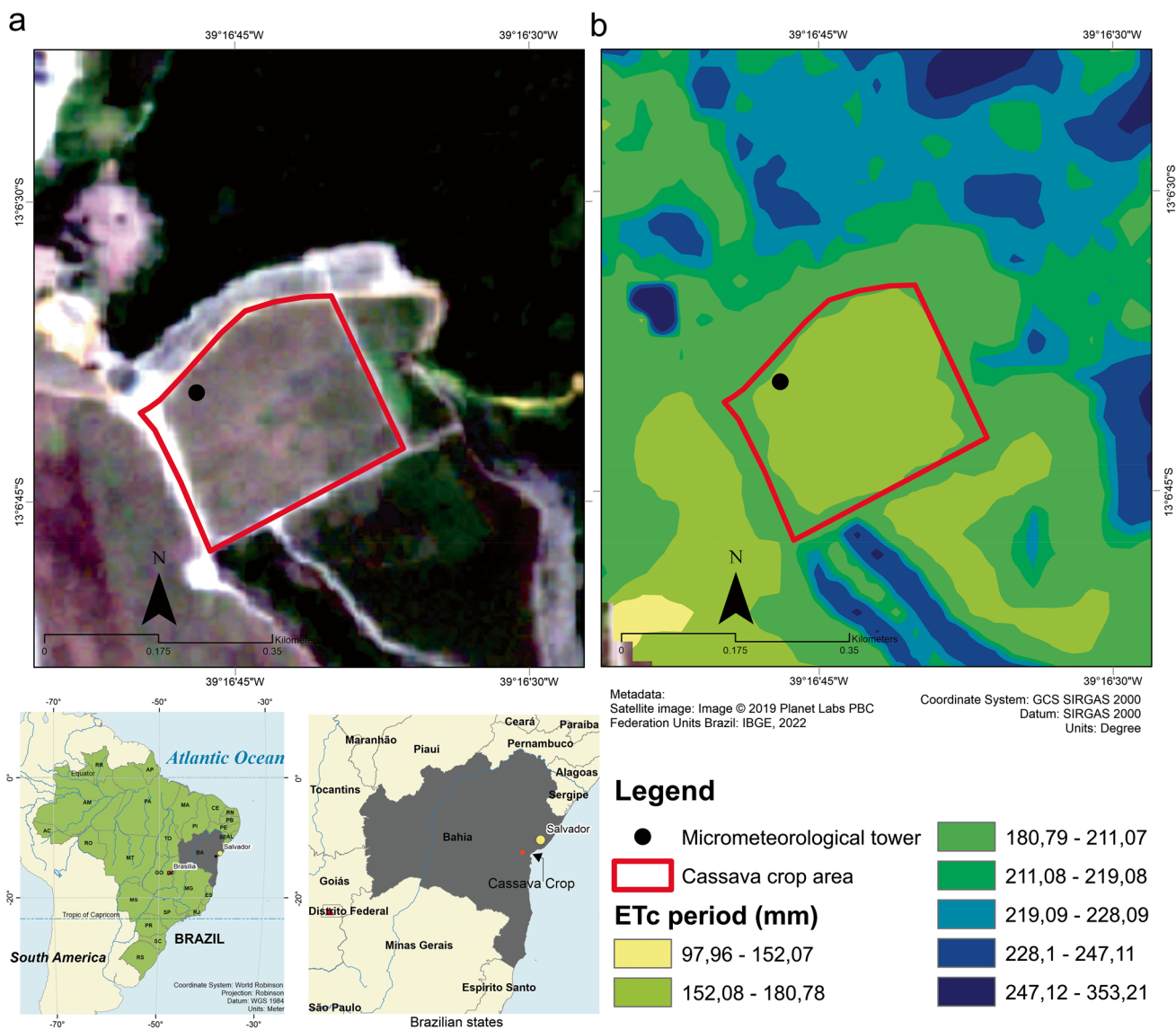


**Fig. 7** (a) Original Planet satellite image (A); (b) Total evapotranspiration a processing cassava field

performance to a specific temperature range since if  $T_s$  does not vary very much, the  $NDVI/T_s$  term will underestimate the  $ETc/R_n$  ratio. Of course, it is necessary to include other types of surfaces when creating the model, followed by a land use map,

updated regularly. Girolimetto and Venturini (2013) found that this relationship ( $NDVI/T_s$ ) can be inversely correlated with a crop moisture index. Nevertheless, another study showed that



it is related to the rate of surface evapotranspiration (Liu; Yao; Wang, 2017; Dijke et al. 2019; Alves et al. 2020;).

Figure 7 presents the total estimated ET<sub>c</sub> maps for the cassava cultivation area. Conversely, significant ET<sub>c</sub> rates were estimated in cassava production fields. The total evapotranspiration by remote sensing simplified (M3) for the period study, ranging from 152 to 180 mm with an average of 160.01 mm, provides an overview of water consumption by the crop during this specific timeframe. This average can serve as a useful benchmark for estimating the water requirements of cassava and for designing appropriate irrigation systems.

The output map generated by through Simplified RS Evapotranspiration (M3) model demonstrates the advantages of utilizing such products for deriving 24-h evapotranspiration estimates for processing cassava crop. This research has significantly enhanced estimation processes by integrating a simplified model with an atmospherically corrected image of evapotranspiration over a 24-h period. Depending on factors such as the type of forest and land cover, the crop stage, and the specific empirical relationships utilized, traditional input parameters used for roughness assessment (such as NDVI, T<sub>s</sub> and LAI). This highlights the importance of advanced models like METRIC, SAFER and other methods, in facilitating remote sensing-based estimation of evapotranspiration for cassava crop, underscoring the need for accurate and comprehensive approaches in agricultural water management.

## 4 Conclusions

The application of combined surface renewal analysis and energy balance (SREB) at the evaporating surface to study the water consumption of a processing cassava field was carried out. Once calibrated against eddy covariance measurements of H, the SREB method demonstrated its potential to accurately determine the crop ET under rainfed conditions in the eastern region of Bahia, Brazil.

Besides the micrometeorological methods, remote sensing techniques were also applied with the METRIC and SAFER algorithms. Due to frequent cloud cover in the area, only three Landsat images from overpasses in May and June could be used. High agreement in terms of crop ET was found between the surface and the remote sensing methods. For the three images, METRIC and SAFER were 8.6% and 26.4% higher than SREB, on average. Such results demonstrate the potential of remote sensing methods for crop ET and water resources management in the study area.

Among the proposed regression models (M1, M2, and M3) for estimation of processing cassava ET, M3 showed a better adjustment with the highest coefficient of determination ( $r^2=0.952$ ) and lowest error (RMSE=0.205 mm day<sup>-1</sup>). In the M3 model, ET/R<sub>n</sub> was expressed as a function of the NDVI/LAI ratio. These three biophysical parameters, R<sub>n</sub>,

NDVI, and LAI, can routinely be determined from image processing for field applications in water management. Therefore, with a limited set of variables, this approach can be satisfactorily applied using data collection methodologies that provide enhanced temporal and spatial resolution.

**Acknowledgements** This research was conducted with the invaluable support of the Coordination for the Improvement of Higher Education Personnel (CAPES), the Foundation for Research and Support of Bahia (FAPESB) with protocol BOL0321/2017, and Embrapa Cassava and Tropical Fruits (EMBRAPA). Financial backing was provided by CNPq through grant/research 311318/2022-3, coordinated by MACF, as well as FAPED (Research Project: FAPED/CNPTIA/BCB\_ZARC/CNPMF-23800.22/0109-7), also under the coordination of MACF. We extend our sincere gratitude to these institutions for their vital contributions to the successful completion of this work.

**Author contributions and participate** All authors contributed to the study conception and design. Material preparation, data collection and analysis were performed by Neilon Duarte da Silva, Aureo Silva de Oliveira and Mauricio Antonio Coelho Filho. The first draft of the manuscript was written by Neilon Duarte da Silva, and all authors commented on previous versions of the manuscript. All authors read and approved the final manuscript.

**Funding** This work was supported by Coordination for the Improvement of Higher Education Personnel (CAPES), the Foundation for Research and Support of Bahia (FAPESB) with protocol BOL0321/2017, and Embrapa Cassava and Tropical Fruits (EMBRAPA). Financial backing was provided by CNPq through grant/research 311318/2022-3, coordinated by MACF, as well as FAPED (Research Project: FAPED/CNPTIA/BCB\_ZARC/CNPMF-23800.22/0109-7).

**Data availability** The datasets generated during and/or analysed during the current study are not publicly available due to as they are source of the University Federal of the Reconcavo of Bahia but are available from the corresponding author on reasonable request..

**Code availability** Not applicable.

## Declarations

**Ethics approval** Not applicable.

**Consent for publication** The authors agree with the publication of the article and are responsible for the content.

**Competing interests** Author Neilon Duarte da Silva, Aureo Silva de Oliveira and Mauricio Antonio Coelho Filho, declare they have no financial interests. The authors have no relevant financial or non-financial interests to disclose.

## References

- Allen R, Irmak A, Trezza R, Hendrickx JMH, Bastiaanssen W, Kjaersgaard J (2011) Satellite-based ET estimation in agriculture using SEBAL and METRIC. *Hydrological Process* 25(26):4011–4027. <https://doi.org/10.1002/hyp.8408>

- Allen RG (1996) Assessing Integrity of Weather Data for Reference Evapotranspiration Estimation. *J Irrig Drain Eng* 122:97–106. [https://doi.org/10.1061/\(asce\)0733-9437\(1996\)122:2\(97\)](https://doi.org/10.1061/(asce)0733-9437(1996)122:2(97))
- Allen RG, Tasumi M, Morse A et al (2007a) Satellite-Based Energy Balance for Mapping Evapotranspiration with Internalized Calibration (METRIC)—Applications. *J Irrig Drain Eng* 133:395–406. [https://doi.org/10.1061/\(asce\)0733-9437\(2007\)133:4\(395\)](https://doi.org/10.1061/(asce)0733-9437(2007)133:4(395))
- Allen RG, Tasumi M, Trezza R (2007b) Satellite-Based Energy Balance for Mapping Evapotranspiration with Internalized Calibration (METRIC)—Model. *J Irrig Drain Eng* 133:380–394. [https://doi.org/10.1061/\(asce\)0733-9437\(2007\)133:4\(380\)](https://doi.org/10.1061/(asce)0733-9437(2007)133:4(380))
- Allen RG, Pereira L, Raes D, Smith M (1998) Crop evapotranspiration guidelines for computing crop requirements. *FAO Irrig. Drain Report Modeling and Application*. *J Hydrol* 285:19–40
- Allen RG (2015) Manual REF-ET version Windows 4.1. Available online at <https://www.uidaho.edu/cals/kimberly-research-and-extension-center/research/water-resources/ref-et-software>. Accessed 10 Mar 2019
- Alvares CA, Stape JL, Sentelhas PC, de Moraes Gonçalves JL, Sparovek G (2013) Köppen's climate classification map for Brazil. *Meteorol Z* 22(6):711–728. <https://doi.org/10.1127/0941-2948/2013/0507>
- da Alves ÉS, Filgueiras R, Rodrigues LN et al (2020) Water stress coefficient determined by orbital remote sensing techniques. *Revista Brasileira de Engenharia Agrícola e Ambiental* 24:847–853. <https://doi.org/10.1590/1807-1929/agriambi.v24n12p847-853>
- Attarod P, Komori D, Hayashi K et al (2005) Comparison of the Evapotranspirations among a Paddy Field, Cassava Plantation and Teak Plantation in Thailand. *J Agric Meteorol* 60:789–792. <https://doi.org/10.2480/agrmet.789>
- Bastiaanssen WGM (2000) SEBAL-based sensible and latent heat fluxes in the irrigated Gediz Basin, Turkey. *J Hydrol* 229:87–100. [https://doi.org/10.1016/S0022-1694\(99\)00202-4](https://doi.org/10.1016/S0022-1694(99)00202-4)
- Bastiaanssen WGM, Menenti M, Feddes RA, Holtslag AAM (1998a) A remote sensing surface energy balance algorithm for land (SEBAL). 1 Formulation. *J ogy* 212–213:198–212. [https://doi.org/10.1016/S0022-1694\(98\)00253-4](https://doi.org/10.1016/S0022-1694(98)00253-4)
- Bastiaanssen WGM, Pelgrum H, Wang J et al (1998b) A remote sensing surface energy balance algorithm for land (SEBAL). 2 Validation. *J Hydrol* 212–213:213–229. [https://doi.org/10.1016/S0022-1694\(98\)00254-6](https://doi.org/10.1016/S0022-1694(98)00254-6)
- Bezerra BG, Bezerra JRC, da Silva BB, dos Santos CAC (2015) Surface energy exchange and evapotranspiration from cotton crop under full irrigation conditions in the Rio Grande do Norte State, Brazilian Semi-Arid. *Bragantia* 74:120–128. <https://doi.org/10.1590/1678-4499.0245>
- Boegh E, Soegaard H (2004) Remote sensing based estimation of evapotranspiration rates. *Int J Remote Sens* 25:2535–2551. <https://doi.org/10.1080/01431160310001647975>
- Burba G (2013) Eddy Covariance Method for Scientific, Industrial, Agricultural and Regulatory Applications. *LI-COR Biosciences*
- Cao Z, Mackay MD, Spence C, Fortin V (2018) Variational Computation of Sensible and Latent Heat Flux over Lake Superior. *J Hydrometeorol* 19:351–373. <https://doi.org/10.1175/jhm-d-17-0157.1>
- Coaguila DN, Hernandez FBT, de Teixeira AH, C, et al (2017) Water productivity using SAFER - Simple Algorithm for Evapotranspiration Retrieving in watershed. *Revista Brasileira De Engenharia Agrícola e Ambiental* 21:524–529. <https://doi.org/10.1590/1807-1929/agriambi.v21n8p524-529>
- Coelho Filho MA (2020). Irrigação da Cultura da Mandioca. Cruz das Almas: Embrapa. (Technical Release 172). 1-12
- Dijke HV, AJ, Mallick K, Teuling AJ et al (2019) Does the Normalized Difference Vegetation Index explain spatial and temporal variability in sap velocity in temperate forest ecosystems? *Hydrol Earth Syst Sci* 23:2077–2091. <https://doi.org/10.5194/hess-23-2077-2019>
- Embrapa - Congresso de Mandioca, 2018. Disponível em: <https://www.embrapa.br/congresso-de-mandioca-2018/mandioca-em-numeros>. Acesso em: 10 de outubro de 2019.
- Folhes MT, Rennó CD, Soares JV (2009) Remote sensing for irrigation water management in the semi-arid Northeast of Brazil. *Agric Water Manag* 96:1398–1408. <https://doi.org/10.1016/j.agwat.2009.04.021>
- Foltynová L, Fischer M, McGloin RP (2019) Recommendations for gap-filling eddy covariance latent heat flux measurements using marginal distribution sampling. *Theoret Appl Climatol* 139:677–688. <https://doi.org/10.1007/s00704-019-02975-w>
- Gao L, Zhao P, Kang S et al (2020) Comparison of evapotranspiration and energy partitioning related to main biotic and abiotic controllers in vineyards using different irrigation methods. *Front Agric Sci Eng* 7:490. <https://doi.org/10.15302/j-fase-2019310>
- Gillies RR, Kustas WP, Humes KS (1997) A verification of the “triangle” method for obtaining surface soil water content and energy fluxes from remote measurements of the Normalized Difference Vegetation Index (NDVI) and surface e. *Int J Remote Sens* 18:3145–3166. <https://doi.org/10.1080/014311697217026>
- Girolimetto D, Venturini V (2013) Water Stress Estimation from NDVI-Ts Plot and the Wet Environment Evapotranspiration. *Adv Remote Sens* 02:283–291. <https://doi.org/10.4236/ars.2013.24031>
- González-Dugo MP, González-Piqueras J, Campos I, Andréu A, Balbontín C, Calera A (2012) Evapotranspiration monitoring in a vineyard using satellite-based thermal remote sensing. *SPIE Proceedings*. <https://doi.org/10.1117/12.974731>
- González-Piqueras J, Villodre J, Campos Rodríguez I, et al (2015) Seguimiento de los flujos de calor sensible y calor latente en vid mediante la aplicación del balance de energía METRIC. *Revista de Teledetección* 43. <https://doi.org/10.4995/raet.2015.2310>
- Hernandez FBT, Neale CMU, de C. Teixeira AH, Taghvaeian S (2014) Determining large scale actual evapotranspiration using agro-meteorological and remote sensing data in the Northwest of Sao Paulo State, Brazil. *Acta Horticulturae* 263–270. <https://doi.org/10.17660/actahortic.2014.1038.31>
- Holwerda F, Guerrero-Medina O, Meesters AGCA (2021) Evaluating surface renewal models for estimating sensible heat flux above and within a coffee agroforestry system. *Agric for Meteorol* 308–309:108598. <https://doi.org/10.1016/j.agrformet.2021.108598>
- Hu Y, Buttar NA, Tanny J et al (2018) Surface Renewal Application for Estimating Evapotranspiration: A Review. *Advances in Meteorology* 2018:1–11. <https://doi.org/10.1155/2018/1690714>
- Jensen ME, Allen RG (eds) (2016) *Evaporation, Evapotranspiration, and Irrigation Water Requirements*. <https://doi.org/10.1061/9780784414057>
- Karnieli A, Agam N, Pinker RT et al (2010) Use of NDVI and Land Surface Temperature for Drought Assessment: Merits and Limitations. *J Clim* 23:618–633. <https://doi.org/10.1175/2009jcli2900.1>
- Koyo P, Hu J, Amou M (2020) Analysis of Spatiotemporal Features of Cassava Evapotranspiration in Benin Using Integrated FAO-56 Method and Terra/MODIS Data. *J Agric Sci* 12:106. <https://doi.org/10.5539/jas.v12n8p106>
- de Lima JRS, Antonino ACD, de Lira CABO, de Souza ES, de da Silva IF (2011) Balanço de energia e evapotranspiração de feijão caupi sob condições de sequeiro. *Revista Ciência Agronômica* 42(1):65–74. <https://doi.org/10.1590/S1806-66902011000100009>
- de Lima JRS, Antonino ACD, de Soares WA, Borges E, da da Silva IF, de Lira CABO (2005) Balanço de energia em um solo cultivado com feijão caupi no brejo paraibano. *Revista Brasileira de Engenharia Agrícola e Ambiental* 9(4):527–534. <https://doi.org/10.1590/S1415-43662005000400014>
- Liu Z, Yao Z, Wang R (2017) Evaluating the surface temperature and vegetation index (Ts/VI) method for estimating surface soil

- moisture in heterogeneous regions. *Hydrol Res* 49:689–699. <https://doi.org/10.2166/nh.2017.079>
- McElrone AJ, Shapland TM, Calderon A et al (2013) Surface renewal: an advanced micrometeorological method for measuring and processing field-scale energy flux density data. *J vis Exp*. <https://doi.org/10.3791/50666-v>
- Mekhmandarov Y, Pirkner M, Dicken U, Tanny J (2012) Examination of the surface renewal technique for sensible heat flux estimates in screenhouses. *Acta Horticulturae* 923–929. <https://doi.org/10.17660/actahortic.2012.952.117>
- Neves LO, Costa JMN, Andrade VM, Lôla AC, Ferreira WP (2008). Energy balance in a cowpea beans (*Vigna unguiculata* L.) crop in the state of Pará. *Revista Brasileira de Agrometeorologia* 16(1):21–30.
- Ortega-Salazar S, Ortega-Farías S, Kilic A, Allen R (2021) Performance of the METRIC model for mapping energy balance components and actual evapotranspiration over a superintensive drip-irrigated olive orchard. *Agric Water Manag* 251:106861. <https://doi.org/10.1016/j.agwat.2021.106861>
- Parry CK, Shapland TM, Williams LE et al (2019) Comparison of a stand-alone surface renewal method to weighing lysimetry and eddy covariance for determining vineyard evapotranspiration and vine water stress. *Irrig Sci* 37:737–749. <https://doi.org/10.1007/s00271-019-00626-6>
- Paw UKT, Qiu J, Su H-B, Watanabe T, Brunet Y (1995) Surface renewal analysis: a new method to obtain scalar fluxes. *Agric Forest Meteorol* 74(1–2):119–137. [https://doi.org/10.1016/0168-1923\(94\)02182-j](https://doi.org/10.1016/0168-1923(94)02182-j)
- Perez-Priego O, El-Madany TS, Migliavacca M et al (2017) Evaluation of eddy covariance latent heat fluxes with independent lysimeter and sapflow estimates in a Mediterranean savannah ecosystem. *Agric For Meteorol* 236:87–99. <https://doi.org/10.1016/j.agrfor.2017.01.009>
- Pôças I, Paço TA, Cunha M et al (2014) Satellite-based evapotranspiration of a super-intensive olive orchard: Application of METRIC algorithms. *Biosys Eng* 128:69–81. <https://doi.org/10.1016/j.biosystemseng.2014.06.019>
- Santos JEO, da Cunha FF, Filgueiras R et al (2020) Performance of SAFER evapotranspiration using missing meteorological data. *Agric Water Manag* 233:106076. <https://doi.org/10.1016/j.agwat.2020.106076>
- Shapland TM, McElrone AJ, Snyder RL, Paw UKT (2012a) Structure Function Analysis of Two-Scale Scalar Ramps. Part I: Theory and Modelling. *Bound-Layer Meteorol* 145:5–25. <https://doi.org/10.1007/s10546-012-9742-5>
- Shapland TM, Snyder RL, Smart DR, Williams LE (2012b) Estimation of actual evapotranspiration in winegrape vineyards located on hillside terrain using surface renewal analysis. *Irrig Sci* 30:471–484. <https://doi.org/10.1007/s00271-012-0377-6>
- Snyder RL, Spano D, Pawu KT (1996) Surface renewal analysis for sensible and latent heat flux density. *Bound-Layer Meteorol* 77:249–266. <https://doi.org/10.1007/bf00123527>
- Su Z (2002) The Surface Energy Balance System (SEBS) for estimation of turbulent heat fluxes. *Hydrol Earth Syst Sci* 6:85–100. <https://doi.org/10.5194/hess-6-85-2002>
- Sun Z, Wei B, Su W et al (2011) Evapotranspiration estimation based on the SEBAL model in the Nansi Lake Wetland of China. *Math Comput Model* 54:1086–1092. <https://doi.org/10.1016/j.mcm.2010.11.039>
- Tasumi M (2019) Estimating evapotranspiration using METRIC model and Landsat data for better understandings of regional hydrology in the western Urmia Lake Basin. *Agric Water Manag* 226:105805. <https://doi.org/10.1016/j.agwat.2019.105805>
- Teixeira AHC (2010) Determining regional actual evapotranspiration of irrigated crops and natural vegetation in the são francisco river basin (Brazil) using remote sensing and penman-monteith equation. *Remote Sensing* 2:1287–1319. <https://doi.org/10.3390/rs0251287>
- Teixeira A, Padovani C, Andrade R et al (2015a) Use of MODIS Images to Quantify the Radiation and Energy Balances in the Brazilian Pantanal. *Remote Sensing* 7:14597–14619. <https://doi.org/10.3390/rs71114597>
- Teixeira AHC, Andrade RG, Leivas JF (2015b) Energy and mass transfer parameters in a brazilian semi-arid ecosystem under different thermohydrological conditions. *Revista Brasileira de Meteorologia* 30:381–393. <https://doi.org/10.1590/0102-778620140101>
- Teixeira AHC, Leivas JF, Andrade RG, Hernandez FBT (2015c) Water productivity assessments with landsat 8 images in the nilo coelho irrigation scheme. *IRRIGA* 1:01–10. <https://doi.org/10.15809/irriga.2015v1n2p01>
- Van Atta CW (1977) Effect of coherent structures on structure functions of temperature in the atmospheric boundary layer. *Archiwum Mechaniki Stosowanej* 29(1):161–171
- Zapata N, Martínez-Cob A (2001) Estimation of sensible and latent heat flux from natural sparse vegetation surfaces using surface renewal. *J Hydrol* 254:215–228. [https://doi.org/10.1016/s0022-1694\(01\)00495-4](https://doi.org/10.1016/s0022-1694(01)00495-4)
- Zapata N, Martínez-Cob A (2002) Evaluation of the surface renewal method to estimate wheat evapotranspiration. *Agric Water Manag* 55:141–157. [https://doi.org/10.1016/s0378-3774\(01\)00188-3](https://doi.org/10.1016/s0378-3774(01)00188-3)
- Zhou S, Wang J, Liu J et al (2011) Evapotranspiration of a drip-irrigated, film-mulched cotton field in northern Xinjiang, China. *Hydrol Process* 26:1169–1178. <https://doi.org/10.1002/hyp.8208>

**Publisher's Note** Springer Nature remains neutral with regard to jurisdictional claims in published maps and institutional affiliations.

Springer Nature or its licensor (e.g. a society or other partner) holds exclusive rights to this article under a publishing agreement with the author(s) or other rightsholder(s); author self-archiving of the accepted manuscript version of this article is solely governed by the terms of such publishing agreement and applicable law.